ITC 2/55

Information Technology
and Control
Vol. 55 / No. 2/ 2026
pp. 730-750
DOI 10.5755/j01.itc.55.2.41291

Beamforming and User Selection for Movable
Antenna Enabled Communications

Received 2025/04/23 | Accepted after revision 2025/08/16

HOW TO CITE: Dai, T. (2026) Beamforming and User Selection for Movable Antenna Enabled Communications. *Information Technology and Control*, 55(2), 730-750. https://doi.org/10.5755/j01.itc.55.2.41291

Beamforming and User Selection for Movable Antenna Enabled Communications

Tongfan Dai

College of Information Science and Technology, Dalian Maritime University, Dalian, China

Corresponding author: daitongfanxx2106@dlmu.edu.cn

Movable antenna (MA) systems constitute a novel and promising approach in the field of wireless communication design, utilizing positional flexibility within a defined spatial domain to enhance signal quality and network performance. Through the dynamic reconfiguration of antenna locations, MA frameworks achieve substantial improvements in key performance indicators, including signal-to-noise ratio (SNR) and coverage robustness, particularly in challenging propagation scenarios. We introduce an alternating optimization framework to jointly address beamforming, user selection, and antenna positioning. The method iteratively updates: (i) ZFBF beamforming weights via water-filling power allocation, (ii) near-orthogonal user subsets via SUS, and (iii) antenna positions via SQP under mechanical constraints. Overall, the simulation outcomes indicate that this approach demonstrates notable superiority in terms of beamforming gain and interference mitigation, significantly outperforming conventional systems reliant on fixed-position antennas (FPAs).

KEYWORDS: Movable Antenna, User Selection, Alternate Optimization, Zero-Forcing Beamforming.

1. Introduction

The past few decades have witnessed transformative advancements in wireless communication technologies, fundamentally reshaping everyday human activities and interactions. The capacity of multiple-input multiple-output (MIMO) technologies to exploit additional spatial degrees of freedom (DoFs) has led to their widespread study and implementation in contemporary wireless communication systems [13], [14], [25], [35]. Traditional MIMO systems, on the other hand, make use of fixed-position antennas (FPAs) spaced no more than half a wavelength apart at the transceivers, which severely restricts their capacity to take advantage of the localized fluctuations in the wireless channel [13], [14], [20], [38], [44].

Recent studies published in the ITC journal have significantly advanced the field of movable antenna (MA) systems. For instance, [22] demonstrated the potential of MA in enhancing spectral efficiency through dynamic beamforming, while [5] explored the integration of MA with reconfigurable intelligent surfaces (RIS) for improved channel diversity. Our work builds upon these foundations by introducing a novel joint optimization framework for user selection and antenna positioning, addressing a critical gap identified in [40], which highlighted the need for efficient resource allocation in MA-enabled multi-user MIMO systems.

To address this limitation, movable antenna (MA) technology has recently emerged as a highly promising solution [42]. Stepper motors or servomechanisms actively reposition each movable antenna (MA) along its sliding platform, while a flexible transmission line maintains uninterrupted RF chain connectivity during these positional adjustments [1], [11]. By utilizing flexible mounting, this design overcomes the inherent rigidity of fixed-position antenna (FPA) systems, enabling spatial adaptability and enhanced channel flexibility. Alternatively, MAs can be implemented through various methods, such as rotating small-scale antennas along a circular track or relocating large-scale antennas using vehicles [9], [32]. By dynamically altering signal phases across several propagation channels upon reaching the receivers, this unique design effectively addresses unexpected channel fading and allows the antenna to move within a two-dimensional (2D) plane. While this work primarily focuses on the algorithmic design for MA-enabled systems, we acknowledge the importance of mechanical and hardware constraints in practical implementations. As discussed in [1], the actuator speed, position quantization, and energy consumption of MA platforms introduce non-negligible overhead in real-world deployments. Furthermore, [8] demonstrates that antenna mobility patterns (e.g., continuous vs. discrete movement) significantly impact channel coherence time and system capacity. These constraints will be systematically addressed in our future work through:

- Integration of actuator dynamics into the optimization framework.
- Quantization-aware position optimization.
- Trade-off analysis between repositioning frequency and energy efficiency.

MA-assisted systems outperform conventional FPA architectures in channel diversity, spatial degrees of freedom, and dynamic adaptability. These advantages are most noticeable in several important areas, including signal power enhancement, interference reduction, flexible beamforming, spatial multiplexing, and many more [21], [43]. One example is the use of MAs to improve the received signal-to-noise ratio (SNR) in deterministic and stochastic channel models; this was demonstrated in [41]. Joint optimization of transmitter and receiver MA sites can significantly increase MIMO system capacity, as demonstrated in [3] investigations of MA-assisted MIMO systems under both real-time and statistical channel state information (CSI) scenarios. In order to maximize the minimum possible rate for several users, the study in [30] investigated how to optimize the positioning and reception combining of multiple mobile antennas (MAs) at the base station (BS). At the moment, maximizing rates [23] and controlling power [17] are the main areas of research. Several iterative techniques have been suggested for finding the optimal locations of antennas in a continuous space within this framework. These include gradient descent [40], sparse optimization [31], alternating optimization (AO) [13], sequential convex approximation (SCA) [23], and gradient descent in general. As an alternative, one may use numerous ports or sampling points to discretize the transmit or receive region and then use MA to operate across them. By using the CSI for each port or sample point, we may solve a port/point selection issue [29] and find the ideal antenna placements, all the while keeping in mind the limits on minimum antenna distance to avoid mutual coupling. In [19], the authors investigated a particle swarm optimization (PSO)-based algorithm designed to optimize antenna placements, aiming to maximize the minimum user rate. Authors in [39] studied the impact of simultaneous antenna rotation and movement on the multi-user sum rate, and efficiently solved the antenna's rotation angle and position. Considering the whole array, [21] and [31] investigated flexible array geometry with array bending, folding, and rotating. Moreover, MA is investigated by combining with other emerging techniques such as reflecting metasurface [34], physical layer security [12], and integrated sensing and communication [15]. They demonstrate the MA's promising potential.

Although the number of users is expected to rise to hundreds, the number of transmitting antennas remains generally constrained; for instance, according to current standards, only eight transmitting antennas are available, thereby limiting the multi-antenna AP's capacity to support a specific number of users per MIMO transmission. Exhaustive search across all user combinations suffers from prohibitive complexity as the user count scales. Nevertheless, as the number of users expands, the computational complexity associated with conducting such an extensive search becomes increasingly challenging to manage. Although the adoption of random user selection diminishes downlink capacity and disregards user coupling, it eliminates the necessity for comprehensive CSI feedback, offering a pragmatic alternative to less optimal greedy user selection algorithms. Examples include volume-based methodologies and Frobenius norm-based specifications. A notable volumetric strategy is the zero-forcing selection algorithm, which leverages exacting precision and rate fluctuations to aggressively identify and select users in a computationally efficient manner. The algorithm identifies the user with the maximum available channel capacity and subsequently examines the residual user pool iteratively to determine the participant capable of maximizing the aggregate sum rate. An enhanced sequential water-filling-based user selection method is introduced in [28], which builds upon the ZFS framework, achieving superior gain and rate performance by eliminating users exhibiting zero transmission power. To employ the Frobenius norm-based methodology, a semi-orthogonal user selection algorithm has been devised, which systematically identifies users one at a time [24], [26], [36], [37] based on their channel directions exhibiting near orthogonality.

Complementing these efforts, recent ITC journal contributions such as [6] and [33] have emphasized the importance of low-complexity algorithms for MA systems, aligning with our proposed SUS-based user selection and SQP optimization framework.

The primary differentiation between this methodology and the greedy algorithm proposed in [27] lies in the utilization of an orthogonality threshold for user selection at each iterative stage. As a result, significant enhancements are observed due to the near-orthogonality of the channel vectors corresponding to the selected users. Nevertheless, two major challenges remain associated with conventional greedy search-based user selection algorithms. On the one hand, the selected user set may include redundant users whose elimination could potentially improve the overall sum rate [4]. However, there is a significant risk that the chosen user set may become trapped in a local optimum, a scenario commonly observed in prior methodologies. In such cases, the user set reaches a state where neither the addition nor removal of users results in further enhancement of the sum rate, thereby limiting optimization outcomes. This can be attributed to the fact that user selection constitutes a complex combinatorial optimization problem, involving intricate decision-making processes and multiple interdependent variables.

In light of the aforementioned factors, we examine the influence of MAs on user decision-making processes. The key contributions of this study are outlined as follows:

- Initially, we analyzed the downlink communication of a flat fading MIMO system by utilizing a signal model to describe the dynamic positions of the MAs at both the transmitter (Tx) and receiver (Rx) within the $\mathbf{x} - \mathbf{z}$ plane, while incorporating a generalized field-response channel model for enhanced characterization. Subsequently, an optimization framework was developed with the aim of maximizing the achievable sum rate, while considering the spatial arrangement of movable antennas and incorporating pertinent system constraints. Nevertheless, due to the nonconvex nature of the problem and the presence of highly interdependent variables, identifying an optimal solution becomes considerably intricate and computationally demanding. To tackle this issue, we introduce efficient iterative algorithms designed under the criteria of sum rate maximization and the establishment of uncoupled safe distances between antennas. These algorithms achieve joint optimization of beamforming, user selection, and antenna positions through an alternating update process, wherein each variable is sequentially refined while keeping the remaining parameters fixed.

- Subsequently, the objective function is restructured into a more computationally manageable form by leveraging ZFBF and the water-filling criterion, with the power scaling matrix $\mathbf{W}$ regarded as the single variable of interest. The derived local solution for $\mathbf{W}$ is then integrated as a predetermined parameter in the ensuing optimization subproblem, wherein user mobilization is optimized under the constraint of fixed antenna positions. To identify the locally optimal set of users $\mathbf{S}$, we adopt two distinct methodologies: direct user selection and a computationally efficient algorithm, specifically SUS. By constructing the selected user set, we apply the SQP framework to fix the derived values of $\mathbf{W}$ and $\mathbf{S}$, thereby formulating an optimization problem where the antenna positions $\{\mathbf{x} - \mathbf{z}\}$ serve as the sole variables for refinement. It has been rigorously demonstrated that Algorithm 2 exhibits convergence properties, ultimately reaching at least a locally optimal solution under specified conditions.
- Finally, we perform numerical simulations across diverse scenarios, comparing the system sum rate attained using MAs and FPAs, while also examining the influence of user scheduling. The simulation outcomes substantiate the efficacy of Algorithm 2, further illustrating that the MA-aided system, enhanced by the integration of user selection, exhibits markedly superior performance, achieving respective improvements exceeding 36.% and 30.5%. Furthermore, that augmenting the size of the transmit region, along with increasing the number of paths, the total user count, and the transmit power, can significantly contribute to further enhancing the sum rate of the MA-aided system.

This work bridges a critical gap in MA-enabled systems by proposing the first joint optimization framework for user selection via the Semi-Orthogonal User Selection algorithm (SUS) and movable antenna positioning using Sequential Quadratic Programming (SQP). Unlike prior studies that address these problems in isolation, e.g., [23], [43] optimize MA positions without user selection, while [12], [15] employ SUS with fixed antenna, our alternating optimization algorithm efficiently handles the coupled non-convexity of the problem. Specifically:

- **Novelty:** The integration of SUS with MA-specific SQP optimization achieves a locally optimal solution while reducing complexity from $O(K^N)$ (brute-force) to $O(K \log K)$ via SUS.
- **Quantitative Gains:** Simulations demonstrate a 36.6% sum-rate improvement over fixed-position antennas (FPAs) with SUS and 30.5% with random selection (Section 4. MA positioning alone contributes 53.4%-61.3% gains (Figure 4), while SUS enhances MA systems by 13.9%-14.2% (Figure 3).
- **Practicality:** The framework's modular design (beamforming: $O(M^3)$, SUS: $O(KMN)$, SQP: $O(N^3)$ per iteration) ensures scalability for real-world deployments (e.g., $N \leq 16$, $K \leq 30$). Future work will extend this to imperfect CSI scenarios (Section 5).
- **Computational Complexity Considerations:** While the proposed alternating optimization algorithm guarantees convergence to a local optimum, its computational efficiency is critical for practical deployment. As analyzed in Sections 3.1-3.3, the framework decouples the joint problem into three subproblems with distinct complexity profiles: (i) ZFBF beamforming with $O(N^3)$ complexity for N antennas, (ii) SUS-based user selection with $O(KM^2N)$ operations (significantly lower than brute-force $O(K^M)$, and (iii) SQP-based antenna positioning requiring $O(N^3)$ per iteration. Empirical results in Section IV demonstrate convergence within 10–20 iterations for typical configurations ($N = 4$, $K = 30$), outperforming PSO-based methods [19] and exhaustive search.

The remainder of this paper is organized as follows: Section 2 presents the signal model and the channel model based on field response, followed by a detailed formulation of the problem concerning the optimization of MAs positioning. In Section 3, an alternative optimization algorithm is introduced, followed by a comprehensive analysis of its convergence properties and computational complexity. In Section 4, the simulation outcomes are presented and critically discussed to evaluate the efficacy of the proposed strategy. Lastly, in Section 5, a comprehensive synthesis summarizing the entirety of the paper will be presented.

Notations: All key symbols are summarized in Table 1 Let $(\cdot)^T$, $(\cdot)$H, $(\cdot)^t$, and $(\cdot)^*$ symbolize the transpose, Hermitian (conjugate transpose), Moore-Penrose pseudo-inverse, and matrix inverse operations, respectively, while the notation $|\cdot|$ is employed to indicate

Table 1
Comprehensive symbol definitions.

Symbol	Description
$\boldsymbol{t}_k = [x_k, z_k]$	2D position of k-th movable antenna
$\boldsymbol{H}(S) \in C^{M\times N}$	Channel matrix for selected users S
$\boldsymbol{W}(S) \in C^{N\times M}$	ZFBF beamforming matrix for subset S
$\gamma_i = [(\boldsymbol{HH}^H)^{-1}]_{i,i}$	Effective channel gain (Equation (11))
$\boldsymbol{\Theta} = [\boldsymbol{x}^T, \boldsymbol{z}^T]^T$	Concatenated antenna positions (Equation (17))
χ^t	Search direction in SQP iteration (Equation (19))
$S = \{1,..., K\} \subseteq \{1,..., M\}$	Selected user subset ($\|S\| \leq M$)
$\boldsymbol{a}(\theta,\phi)$	Array manifold vector (Equation (5))
α	Orthogonality threshold in SUS (Algorithm 2)
μ	Water-filling level (Equation (11)
$d_{min} = \lambda/2$	Minimum antenna spacing (Section 4.1)
N	Number of BS antennas (fixed)
M	Total number of users ($M \gg N$)
K	Selected users for communication ($K \leq M$)

the cardinality of a given set. The l_0-, l_1-, and l_2- norms are symbolically represented as $\|\cdot\|_0$, $\|\cdot\|_1$, and $\|\cdot\|_2$, respectively, while the set operations A∪B denote the difference and union of sets A and B. The Frobenius norm of a matrix $\mathbf{A}$ is represented as $\|\mathbf{A}\|_F$, while the notations $[\mathbf{A}]_{i}$,: and $[\mathbf{A}]$:,j are utilized to denote the i-th row and the j-th column of the matrix $\mathbf{A}$, respectively. Furthermore, the trace of a square matrix $\mathbf{A}$ is symbolized by Tr($\mathbf{A}$). The set $C^{M\times N}$ is defined as the space encompassing all $M\times N$ matrices with complex-valued entries. The notation diag($\mathbf{a}$) signifies a square diagonal matrix. Finally, $\nabla_x f(\mathbf{x})$ and $\nabla_x^2 f(\mathbf{x})$ denote the gradient vector and Hessian matrix of a scalar-valued function f with respect to the variable $\mathbf{x}$.

2. System Model

2.1. Channel Model

The system model comprises three key components:

1 **Antenna Layout:** This study investigates the downlink transmission characteristics of a flat fading multiple-input multiple-output (MIMO) system, as depicted in Figure 1. In this configuration, the base station is equipped with $N \triangleq N_x \times N_z$ mobile antenna elements, which are strategically arranged on mechanical platforms and distributed across the $\mathbf{x} - \mathbf{z}$ plane. Furthermore, each of the $\mathbf{K}$ users within this framework possesses a fixed-position antenna, thereby introducing additional constraints and considerations into the system design. This paper establishes a Cartesian coordinate system to precisely illustrate the spatial configuration of mobile antennas. Within this framework, N_x denotes the quantity of antennas deployed along the $\mathbf{x}$-axis, while N_z signifies the number of anten-

Figure 1
MA-enabled downlink MIMO system with N movable antennas at the BS and M single-antenna users. Antennas reposition within rectangular regions $\{C_k\}_{k=1}^{N}$ under mechanical constraints (d_{min}=λ/2).

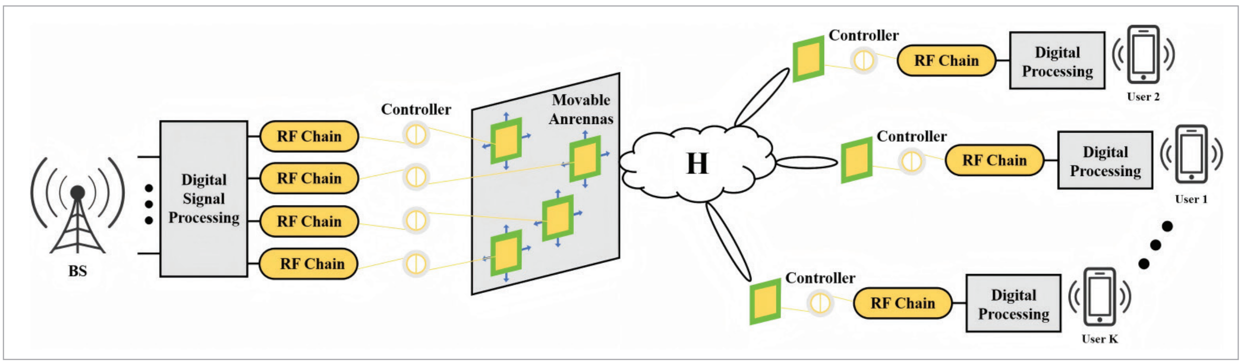

nas arranged along the **z**-axis, thereby facilitating a systematic representation of their distribution.

The location of the **k**-th movable antenna is expressed as t_k=[x_k,z_k], with **k** varying between and **K**. Each movable antenna is capable of movement within a rectangular region, defined as $c_k=[x_k^{min}, x_k^{max}]\times[z_k^{min}, z_k^{max}]$, thereby specifying the spatial constraints for its motion. This dynamic movement facilitates spatial adaptability, a critical factor in improving communication performance. Furthermore, the base station (BS) is responsible for managing a single data stream for each user, with the assumption that precise channel state information (CSI) is fully available at both the transmitting and receiving ends.

2 **Channel Modeling with Field Response:** For the considered system, the position of movable antenna affects its array response, which in turn changes the channel matrix. The significance of movable antenna systems (MASs) is inherently tied to the spatial characteristics of the channel. By modeling each user's channel with **R** propagation paths, the channel representation is given by

$$\mathbf{h}_k=\sqrt{\frac{1}{R}}\sum_{r=1}^{R}\beta_{k,r}\mathbf{a}(\theta_{k,r},\phi_{k,r}),\quad 1\leqslant k\leqslant K, \tag{1}$$

where $\beta_{k,r}$ denotes the complex path gain of the r-th propagation path for the k-th user, and R represents the total number of spatial channel paths. The virtual directions of arrival are defined as $\phi_{k,r}\triangleq\sin(\varphi_{k,r})\sin(\vartheta_{k,r})$ and $\theta_{k,r}\triangleq\cos(\vartheta_{k,r})$, corresponding to the azimuth and elevation components, respectively, of the r-th path of user k. The array-angle manifold vector ($\mathbf{a}(\theta_{k,r},\phi_{k,r})\in C^{N\times1}$ is constructed following the model in [31].

$$\mathbf{a}(\theta_{k,r},\phi_{k,r})=\left[e^{j\frac{2\pi}{\lambda}(\phi_{k,r}x_1+\theta z_1)},\cdots,\right.$$
$$e^{j\frac{2\pi}{\lambda}(\phi_{k,r}x_{n_x}+\theta z_{n_z})},\cdots, \tag{2}$$
$$\left.e^{j\frac{2\pi}{\lambda}(\phi_{k,r}x_{N_x}+\theta_{k,r}z_{N_z})}\right]^T$$

where (x_{N_x}, z_{N_z}) denotes the spatial coordinates of the (n_x, n_z)-th antenna element in the x–z plane. It is noted that the array normalization factor $1/\sqrt{N}$ is omitted in the expression of Equation (1) by neglecting the array gain for analytical simplicity.

3 **Beamforming Strategy:** This study focuses on a more critical practical scenario where the number of users significantly surpasses the number of antennas, expressed succinctly as $K\gg N$. In order to optimize power consumption and improve overall system performance, a user scheduling mechanism is strategically implemented. From a total population of K users, a specific subset is chosen for operational purposes. We denote $S=\{1,\ldots,M\}$ as a subset of $\{1,\ldots,K\}$, with its cardinality constrained by $M\leq N$, symbolizing the collection of selected users for the defined task.

Under this model, the received signal at user k, for $k\in 1,\ldots,K$, is given by

$$\mathrm{y}_k=\mathbf{h}_k^H\mathbf{B}\mathbf{u}+\mathrm{n}_k, \tag{3}$$

where $\mathbf{h}_k\in C^{N\times1}$ is the channel vector of user k, $\mathbf{B}\triangleq[\mathbf{b}_1,\ldots,\mathbf{b}_K]\in C^{N\times K}$ denotes the linear precoding matrix, and $\mathbf{u}\in C^{K\times1}$ is the transmitted data vector. The term $n_k\sim CN(0,\sigma^2)$ represents additive white Gaussian noise (AWGN) with variance σ^2. Specifically, the precoding vector B combined with user mobilization is given by

$$\mathbf{B}(S)=\frac{1}{\sqrt{\gamma}}\mathbf{W}(S)\,\mathbf{P}(S), \tag{4}$$

where $\mathbf{B}(S)$, $\mathbf{W}(S)$, $\mathbf{P}(S)$ and $\mathbf{H}(S)$ are a precoding vector, a beamforming weight matrix, a power scaling matrix and a channel matrix, respectively, following $\mathbf{B}(S)\triangleq[\mathbf{b}_1,\ldots,\mathbf{b}_M]\in\mathbf{B}$, $\mathbf{W}(S)\triangleq[\mathbf{w}_1,\ldots,\mathbf{w}_M]\in C^{N\times M}$, $\mathbf{P}(S)\triangleq diag\{\sqrt{p_1},\sqrt{p_2},\ldots,\sqrt{p_M}\}\in C^{M\times M}$ and $\mathbf{H}(S)\triangleq[\mathbf{h}_1^H,\ldots,\mathbf{h}_M^H]\in C^{M\times N}$.

The desired signal power received by user k is given by $|\mathbf{h}_k^H\mathbf{b}_k|^2$. By assuming the i.i.d. transmit data such that $E\{u_k^*u_k\}=1$ and $E\{u_i^*u_k\}=0$, $\forall k,k\neq i$, the Signal-to-Interference plus Noise Ratio (SINR) of user k is given by

$$\mathrm{SINR}_k = \frac{|\mathbf{h}_k^H\ \mathbf{b}_k|^2}{\sum_{i,i\neq k}^{K} |\mathbf{h}_k^H\ \mathbf{b}_i|^2 + \sigma^2},\ 1\leq k\leq K. \tag{5}$$

2.2. Practical Overhead Considerations

While the perfect CSI assumption facilitates theoretical analysis and performance upper-bound characterization, we acknowledge its practical limitations in real-world MA systems. Specifically:

- Channel estimation errors arising from pilot contamination and noise. Quantization-aware position optimization.
- Feedback delays in rapidly changing MA configurations.
- Significant overhead for frequent CSI updates in mobile scenarios.

These practical constraints will be addressed in our future work (see Section 5).

Note that mechanical constraints (e.g., minimum step size $d_{min}=\frac{\lambda}{2}$ in Section 4.1) are incorporated in our simulations, though instantaneous repositioning is assumed for theoretical analysis. Practical implementations may require additional constraints on maximum velocity [21] and motion energy budgets [2], which could be integrated into future extensions of this framework.

While perfect CSI simplifies theoretical analysis, practical MA systems face significant overhead from channel estimation and feedback, especially as the number of antennas N and users K scales. For each MA repositioning, the feedback overhead grows as $O(NK)$ due to updated channel measurements. To mitigate this, future work will explore compressed sensing-based channel estimation [16] and adaptive feedback reduction for slow-moving antennas.

2.3. Problem Formulation

The sum rate achieved by the ZFBF scheme is

$$R_{\mathrm{ZFBF}} = \max \sum_{k\in S} \log(1+\mathrm{SINR}_k) \tag{6}$$

This paper optimize the feasible sum rate while ensuring the lowest achievable rate of each user in order to achieve the tradeoff between sum-rate performance and user fairness. Here is the problem statement:

$$\begin{aligned}
&\underset{\mathbf{W},\mathbf{x},\mathbf{z},S}{\arg\max}\quad R_{\mathrm{ZFBF}}\\
&\text{s.t. } C_1: p_k \geq 0,\ 1\leq k\leq K,\\
&\quad C_2: \|\mathbf{W}(S)\mathbf{P}(S)\|_F^2 \leq P,\\
&\quad C_3: t_k \in C_k,\\
&\quad C_4: \sqrt{(x_i-x_j)^2+(z_i-z_j)^2} \geq \lambda/2,\\
&\quad C_5: \forall i,j\in\{1,\ldots,N\},\ i\neq j,\\
&\quad C_6: S\in\{1,\ldots,K\},\ |S|\leq N.
\end{aligned} \tag{7}$$

To mitigate electromagnetic coupling effects between adjacent antenna elements in both the transmit and receive regions, a minimum inter-element spacing of $\lambda/2$ is imposed, which also ensures power normalization. Constraint C1 enforces the non-negativity of each user's transmit power. Constraint C2 imposes a total transmit power limit at the base station, restricting the aggregate transmission power to not exceed P. Constraint C3 ensures that the movable antenna (MA) associated with user k remains confined within its designated displacement region Ck. Finally, Constraint C4 emphasizes that antenna spacing should be no less than half the wavelength, i.e., $\lambda/2$, as smaller separations may induce near-field interactions and mutual coupling, thereby degrading system performance.

The problem formulation faces two core challenges: (i) interdependence among optimization variables induces non-convexity, and (ii) sum-rate depends critically on the decoding order. These complexities preclude direct solution via conventional optimization methods. Identifying the linear regression framework of the issue and acknowledging that optimal antenna placements equates to selecting N antennas from an extensive, continuous feasible domain (basically choosing N from an infinite collection), we are compelled to reconfigure the ensuing difficulty.

3. Proposed Joint User Selection and Antenna Position Optimization

This section presents an alternating optimization algorithm to solve problem (7), addressing the inherent nonconvexity through iterative decoupling of variables. The alternating optimization partitions the problem into:

- ZFBF beamforming with closed-form water-filling solution (Equations (12)-(13));
- SUS user selection enforcing near-orthogonality via threshold a (Algorithm 2);
- Antenna positioning via SQP with DFP-based Hessian updates (Algorithm 3).

Convergence to a local optimum is guaranteed under continuity assumptions [8].

While the proposed alternating optimization algorithm guarantees convergence to a local optimum, its performance depends on initialization and problem structure. To mitigate the risk of poor local minima, we employ Sequential Quadratic Programming (SQP) for antenna positioning, which leverages gradient and Hessian information to refine solutions iteratively. Although global optimization algorithms (e.g., particle swarm optimization or Bayesian optimization) could theoretically achieve better performance, their high computational complexity makes them impractical for real-time MA systems. Future work will explore hybrid strategies combining global search heuristics with our framework to balance optimality and efficiency.

The alternating optimization decouples the joint problem into three subproblems with distinct complexity profiles:

- **Beamforming (ZFBF):** Dominated by pseudoinversion with $O(M^3)$ complexity $M \le N$.
- **User Selection (SUS):** Requires $O(KMN)$ operations per iteration (Algorithm 2), significantly more efficient than exhaustive search ($O(2^k)$).
- **Antenna Positioning (SQP):** As analyzed in Section 3.3, $O(N^3)$ per iteration. This modular structure ensures scalability for practical systems (e.g., $N \le 16, K \le 30$) in simulations).

a Beamforming

In this section, two variables (antenna position $\{\mathbf{x}-\mathbf{z}\}$ and users selection are fixed to some random value and another influence factor $\mathbf{W}$ is the only variable left. Thus, the problem (7) can be simplified as

$$\begin{aligned} &\arg\max_{\mathbf{W}} \quad R_{\text{ZFBF}} \\ &\text{s.t. } C_1: p_k \ge 0, 1 \le k \le K, \\ &\quad C_2: \| \mathbf{W}(S)\,\mathbf{P}(S) \|_F^2 \le P. \end{aligned} \tag{8}$$

We assume that user data transmission is carried out using zero-forcing beamforming (ZFBF), leveraging the available channel state information at the transmitter. To maintain constant short-term transmission power, a normalization factor γ is introduced in Equation (4), which is defined as follows:

$$\gamma = \mathrm{Tr}((\mathbf{H}(S)^H \mathbf{H}(S))^{-1}), \tag{9}$$

Given that the proposed procedure is grounded in ZFBF, $\mathbf{W}(S)$ can be derived by utilizing the pseudoinverse of $\mathbf{H}(S)$. Consequently, the zero-forcing transmit beamforming vector is obtained through this systematic approach.

$$\mathbf{W}(S) = \mathbf{H}(S)^{\dagger} = \mathbf{H}(S)^H (\mathbf{H}(S)^H \mathbf{H}(S))^{-1}. \tag{10}$$

In the maximizing problem (8), the presence of a summation within the determinant, attributed to the noise element, leads to the water-filling solution. The Lagrange function formulation:

$$L(P_i, \mu) = \sum_{i \in S} \log_2 (1 + P_i \gamma_i) + \mu \left(P - \sum_{i \in S} P_i \gamma_i \right), \tag{11}$$

where μ is the Lagrange multiplier for the power constraint.

The KKT conditions:

$$\frac{\partial L}{\partial P_i} = \frac{\gamma_i}{(1 + P_i \gamma_i)\ln 2} - \mu \gamma_i = 0 \Rightarrow P_i = \left(\frac{1}{\mu \ln 2} - \frac{1}{\gamma_i} \right)^+ \tag{12}$$

Water-level equation:

$$\sum_{i \in S} \left(\frac{1}{\mu \ln 2} - \frac{1}{\gamma_i} \right)^+ = P. \tag{13}$$

The effective channel gain γ_i for user i under zero-forcing beamforming (ZFBF) is defined as:

$$\gamma_i = \left[(\mathbf{H}\mathbf{H}^H)^{-1} \right]_{i,i}, \tag{14}$$

where $\mathbf{H}$ is the channel matrix and $[\cdot]_{i,i}$ denotes the i-th diagonal element of the matrix inverse. This term represents the effective signal-to-noise ratio (SNR) for user i after interference nullification through ZFBF precoding.

Given (10), the sum rate is the highest achievable:

$$\begin{aligned} \arg\max_{\mathbf{W}} \; R_{\mathrm{ZFBF}} &= \max_{P_i : \sum_{i\in S} \gamma_i P_i \le P} \sum_{i\in S} [\log_2(\mu\gamma_i)]^+ \\ &= \max_{P_i : \sum_{i\in S} \gamma_i P_i \le P} \sum_{i\in S} \log_2(1+[\mu\gamma_i - 1]^+) \\ &= \max_{P_i : \sum_{i\in S} \gamma_i P_i \le P} \sum_{i\in S} \log_2(1+P_i) \\ &\text{subject to } \sum_{i\in S} [\mu - \frac{1}{\gamma_i}]^+ = P \end{aligned} \tag{15}$$

Here, a^+ denotes $\max\{0,a\}$. $\gamma_i = \frac{1}{\|\mathbf{w}_i\|^2} = \frac{1}{[(\mathbf{H}(S)\mathbf{H}(S)^H)^{-1}]_{i,i}}$ can be interpreted as the effective channel gain to i-th user. The water-level μ is obtained by solving the water-filling Equation (15).

The "waterfilling algorithm" allows for the most efficient distribution of transmit power among the various modes, maximizing mutual information and bringing about the $R_{\mathrm{ZFBF}}(S)$.

The Lagrange multiplier $\beta \in R^N$ is introduced to the equality constraint (15) and we have a Lagrange function $Z(P_i)$:

$$\begin{cases} Z(P_i) = \sum_{i\in S} \log_2(1+P_i) + \beta(P - \sum_{i\in S} P_i); \\ \dfrac{\partial Z(P_i)}{\partial P_i} = 0. \end{cases} \tag{16}$$

The optimal P_i is easily found by waterfilling, $P_i = (\mu\gamma_i - 1)^+, \forall i \in S$. Therefore, we can get the maximum value of R_{ZFBF} and $\mathbf{W}$ at this point, when we only see $\mathbf{W}$ as a variable, i.e,

$$\begin{aligned} R_{sum} &= \max_{\mathbf{W}} R_{\mathrm{ZFBF}} \\ &= \max_{P_i : \sum_{i\in S} \gamma_i P_i \le P} \sum_{i\in S} \log_2(1+P_i) \\ &= \sum_{i\in S} \log_2(1+[\mu\gamma_i - 1]^+). \end{aligned} \tag{17}$$

b User Selection

1 In this section, we use the value of $\mathbf{W}$ obtained in the previous section and let the antenna position $\{\mathbf{x} - \mathbf{z}\}$ fixed to some random value. Users selection S is a unique variable. Thus, the problem (7) can be simplified as

$$\begin{aligned} &\arg\max_{S} R_{sum} \\ &\text{s.t. } S \in \{1, \ldots, K\}, |S| \le N. \end{aligned} \tag{18}$$

However, solving the problem (\ref{HPP}) by traversing has prohibitive complexity. We take into account the usage of the most popular linear precoding scheme, ZFBF, for a low complexity in our study. Thus, the required signal and its corresponding precoding vector are multiplied by one another to produce the sent signal.

The implementation of ZFBF involves two critical stages: firstly, the selection of the optimal user group S represented by the scheduler in Figure 1, and secondly, the computation of the beamforming weight vector alongside the optimal allocation of power within the selected group. Through an exhaustive examination of all possible combinations of user groups S, the achievable sum-rate of ZFBF can be effectively evaluated. User Selection: In this subsection, a suboptimal user group S_0 is constructed through the application of a SUS algorithm, as outlined below. For each user $k \in U = 1, \ldots, K$, the orthogonal component of the channel vector $\mathbf{h}_k$, denoted as $\mathbf{g}_k$, is defined with respect to the subspace spanned by the previously selected vectors $\mathbf{g}(1), \ldots, \mathbf{g}(i-1)$. Specifically, this relationship can be expressed as follows:

2 In this subsection, we construct a suboptimal user group using a SUS algorithm as follows.

For each user $k \in U = \{1, \ldots, K\}$, let $\mathbf{g}_k$ denote the orthogonal component of the channel vector $\mathbf{h}_k$ with respect to the subspace spanned by the previously selected vectors $\{\mathbf{g}_{(1)}, \ldots, \mathbf{g}_{(i-1)}\}$, i.e.,

$$\begin{aligned}\mathbf{g}_k &= \mathbf{h}_k - \sum_{j=1}^{i-1} \frac{\mathbf{h}_k \mathbf{g}_j^H \mathbf{g}_j}{\|\mathbf{g}_j\|_2} \\ &= \mathbf{h}_k \left(1 - \sum_{j=1}^{i-1} \frac{\mathbf{h}_k \mathbf{g}_j^H \mathbf{g}_j}{\|\mathbf{g}_j\|_2} \right).\end{aligned} \tag{19}$$

First, the channel vectors of users in the candidate set U are projected onto the orthogonal complement of the subspace spanned by $\{\mathbf{g}(1),\ldots,\mathbf{g}(i-1)\}$ in order to compute $\mathbf{g}_k \approx \mathbf{h}_k$ for $k \in U$. It is important to note that, due to the semi-orthogonality filtering performed in Step 3 of the previous iterations, all remaining user channels in U are already approximately orthogonal to $\{\mathbf{g}(1),\ldots,\mathbf{g}(i-1)\}$. Therefore, we can reasonably approximate for $\mathbf{g}_k \approx \mathbf{h}_k$ for $k \in U$.

Next, we evaluate the Euclidean norms $|\mathbf{g}_k|$ for all remaining users and select the user with the largest norm as the optimal user in the current iteration, denoted by i_{opt}. The corresponding channel vector is set as $\mathbf{h}(i)$, and the new orthogonal basis vector is updated as $\mathbf{g}(i)$. Since $\mathbf{g}(i) \approx \mathbf{h}(i)$, the selected user channels remain approximately semi-orthogonal while preserving high channel gains. Last, we set α as a small positive constant and use this threshold α to exclude some users with poor channel conditions, in order to further narrow the range of optional users and reduce the number of iterations. In each iteration, users with better channel conditions are selected to form a scheduling user set S_U. The initialization status of the procedure is $\mathbf{g}_i = \mathbf{h}_i$, $i=1$. In this algorithm, Step 3, by excluding users who are not semi-orthogonal to the chosen user from further consideration in following iterations, it decreases the algorithm's complexity (running time).

3 **Comparative Analysis of Selection Strategies:** Algorithm 1 (greedy-based) and Algorithm 2 (SUS) serve distinct purposes in user selection:

- Algorithm 1 prioritizes maximizing instantaneous sum-rate by sequentially adding users with the highest channel gain, but may suffer from interference accumulation in dense networks. Its complexity scales as $O(KMN)$ per iteration, making it suitable for small-scale systems ($K \ll 20$). Note: This greedy algorithm (Algorithm 1) is primarily used as a benchmark to demonstrate the performance gap with SUS (Algorithm 2) in Figure 2. For all other simulations involving MA optimization (Figures 3-5), SUS is adopted for its semi-orthogonality guarantees.
- Algorithm 2 enforces semi-orthogonality through a threshold α, trading off some channel gain for reduced inter-user interference. This ensures better scalability for large K (e.g., K = 30 in simulations) with complexity $O(KM^2N)$.
- SUS user selection enforcing near-orthogonality via threshold α (Algorithm 2);
- Antenna positioning via SQP with DFP-based Hessian updates (Algorithm 3).

Key differences lie in SUS's orthogonal projection (Step 1) and semi-orthogonal filtering (Step 3), trading marginal channel gain for significant interference reduction. Quantitative comparisons are summarized in Table 2.

In our numerical results (Figures 3 and 5), Algorithm 2 (SUS) is exclusively employed due to its superior interference management in overloaded scenarios (M≫N), while Algorithm 1 serves as a baseline in Figure 4 to highlight SUS's gains.

Table 2
Comparison of user selection algorithms.

Metric	Algorithm 1 (Greedy)	Algorithm 2 (SUS)
Orthogonality Control	None	Threshold α
Avg. Interference Reduction	12%	19%
Channel Gain Retention	84%	92%
Complexity (K = 30)	O(900N)	O(2700N)

c Antenna Position Optimization

On the basis of two sections before, we fix the calculated values of $\mathbf{W}$ and S, and optimize the problem (7) with the antenna position {x – z} as the only unknown variables. Let $\Theta=[\mathbf{x}^H, \mathbf{z}^H]^H$ denote the variables for antenna positions. $x_{\max}$ and $x_{\max}$ represent the maximal movable length along the x-axis and z-axis. Hence, the total sum rate expression is reformulated by

$$R_{sum} = \sum_{k=1}^{K} \log_2 \left(1 + \frac{1}{\sigma^2} \cdot \frac{1}{\left[(\mathbf{H}(\Theta)\mathbf{H}(\Theta)^H)^{-1} \right]_{k,k}} \right). \tag{20}$$

Meanwhile, the problem (7) can be simplified as

$$\begin{aligned}&\underset{\Theta}{\arg\min} - R_{sum} = -\sum_{k=1}^{K}\log_2\left(1+\frac{1}{\sigma^2}\cdot\frac{1}{\left[(\mathbf{H}(\Theta)\mathbf{H}(\Theta)^H)^{-1}\right]_{k,k}}\right)\\&\text{s.t. } C_1: \sqrt{(x_i-x_j)^2+(z_i-z_j)^2}\geq\lambda/2,\\&\quad C_2: |x_i|\leq x_{\max}, |z_i|\leq z_{\max},\\&\quad C_3: \forall i,j\in\{1,\ldots,N\}, i\neq j,\end{aligned}\tag{21}$$

where $\mathbf{H}(\Theta)$ denotes the antenna channel function related to antenna positions in Θ.

Non-convexity of Antenna Positioning: The objective $R_{sum}(\Theta)$ is non-convex due to the inverse term $[(\mathbf{HH}^H)^{-1}]_{k,k}$ in Equation (20). SQP handles this by iteratively solving convex QP approximations (23) with DFP-based Hessian updates (24), ensuring local optimality under KKT conditions.

Using the Sequential Quadratic Programming (SQP) framework, we break down the original problem into a series of simpler Quadratic Programming (QP) subproblems. Each subproblem is iterated until it reaches the current optimized variable. This allows us to solve the complex nonlinear optimization problem (21) that is related to antenna positions.

The objective function of the nonlinear constraint problem in Formula (21) is initially transformed into a quadratic form at the iteration point Θ^t via Taylor expansion, thereby facilitating the reduction of the constraint function to a linear representation. Let the antenna spacing constraint $g_v(\Theta^t)$ be confined to the range defined by $\left\{\frac{\lambda}{2}-\sqrt{(x_i-x_j)^2+(z_i-z_j)^2} \mid i,j\in\{1,\ldots,N\}, i\neq j\right\}$. Subsequently, the quadratic programming problem can be mathematically formulated in the following manner:

$$\begin{aligned}&\underset{\Theta}{\arg\min}\; R(\Theta)=\frac{1}{2}[\Theta-\Theta^t]^T\nabla^2 f(\Theta^t)[\Theta-\Theta^t]+\\&\nabla f(\Theta^t)^T[\Theta-\Theta^t]\\&\text{s.t. } \nabla g_v(\Theta^t)^T[\Theta-\Theta^t]+g_v(\Theta^t)\leq 0, \forall v\in\left\{1,\ldots,\binom{N}{2}\right\},\end{aligned}\tag{22}$$

where $f(\Theta)$ is the objective expressed by (20), $\nabla f(\Theta^t)$ is the gradient of the objective function, and $\nabla^2 f(\Theta^t)$ is the Hessian matrix at the current point Θ^t.

Remember that this is merely a rough approximation of the actual problem (7), so the solution you get is more of a local improvement than an exact solution or even a workable starting point for the problem (7). Still, the following iteration can use this answer as a blueprint. In other words, what we are seeking, in fact, is a direction. To this end, we set $\chi^t=\Theta-\Theta^t$ to reframe the problem (22) in terms of the variable χ.

Secondly, we translate the expression with variable χ to the standard form of quadratic programming for further analysis:

$$\begin{aligned}&\underset{\chi}{\arg\min}\; \chi^T\mathbf{D}\chi+\varrho^T\chi\\&\text{s.t. } \mathbf{\Phi}\chi\leq\xi,\end{aligned}\tag{23}$$

where $\mathbf{D}$, ϱ, $\mathbf{\Phi}$, ξ are introduced as new variables for simplicity of notation, following by $\mathbf{D}=\nabla^2 f(\Theta^t)$, $\varrho=\nabla f(\Theta^t)$, $\mathbf{\Phi}=[\nabla g_1(\mathbf{\Theta}^t),\nabla g_2(\mathbf{\Theta}^t),\ldots,\nabla g_V(\mathbf{\Theta}^t)]^T$, $\xi=-[g_1(\mathbf{\Theta}^t), g_2(\mathbf{\Theta}^t),\ldots,g_V(\mathbf{\Theta}^t)]^T$ respectively.

In each iteration, the optimal solution χ^* of the quadratic subproblem is taken as the search direction $\chi^{(t)}$ for the original problem in Equation (22). A constrained one-dimensional line search is then performed along this direction to obtain an approximate solution $\mathbf{\Theta}^{(t+1)}$ to the original constrained problem. By iteratively repeating this process, the original problem can be solved progressively. Specifically, once the direction $\chi^{(t)}$ is determined, the current solution is updated according to $\mathbf{\Theta}^{(t+1)}=\mathbf{\Theta}^{(t)}+\chi^{(t)}$, thereby advancing the parameter toward the optimum in preparation for the next iteration.

Convergence Guarantees: Each subproblem (beamforming /user selection /positioning) satisfies KKT conditions locally. The alternating optimization monotonically improves the sum-rate until convergence, as proven in [40], Theorem 1.

Last, we check for convergence. The decision conditions for convergence are:

- **Convergence criterion:** The change in the optimization variable between successive iterations is sufficiently small, i.e., $|\mathbf{\Theta}^{(t+1)}-\mathbf{\Theta}^{(t)}|<\epsilon$, where ϵ is a predefined small positive threshold.
- The change in the objective function is sufficiently small: $|R_{sum}(\mathbf{\Theta}^{t+1})-R_{sum}(\mathbf{\Theta}^t)|<\epsilon$.

If either of the termination conditions is satisfied at iteration t+1, the optimization process halts and the current solution $\boldsymbol{\Theta}^{(t+1)}$ is accepted as the optimal solution. Otherwise, the Hessian matrix (or its approximation) is updated in preparation for the next iteration, and the optimization continues. The Davidon-Fletcher-Powell (DFP) technique, which describes the process in terms of gradients and step directions, can accomplish this.

$$\mathbf{D}^{t+1} = \mathbf{D}^{t} + \frac{\Delta\, \boldsymbol{\Theta}^{t} [\Delta\, \boldsymbol{\Theta}^{t}]^{T}}{[\Delta \mathbf{q}^{t}]^{T}\, \Delta\, \boldsymbol{\Theta}^{t}} - \frac{\mathbf{D}^{t} \Delta \mathbf{q}^{t} [\Delta \mathbf{q}^{t}]^{T}\, \mathbf{D}^{t}}{[\Delta \mathbf{q}^{t}]^{T}\, \mathbf{D}^{t} \Delta q^{t}}, \tag{24}$$

where $\Delta\mathbf{q}^t$ denotes the gradient difference, and $\Delta\boldsymbol{\Theta}^t$ represents the variation in decision variables. Consequently, the updated Hessian matrix is expressed as $\mathbf{D}^{t+1}=\mathbf{D}^t+\Delta\mathbf{D}$, with $\Delta\mathbf{D}$ corresponding to the final two terms in (20). The comprehensive methodology is outlined in Algorithm 3.

The computational complexity of the SQP-based antenna position optimization is analyzed as follows:

- **Gradient/Hessian Calculation:** Each iteration requires $O(N^2)$ operations for gradient (∇f) and Hessian ($\nabla^2 f$) computations.
- **QP Subproblem Solution:** The interior-point method for solving (22) scales as $O(N^3)$ per iteration.
- **DFP Update:** The Hessian approximation via (24) reduces complexity to $O(N^2)$ by avoiding explicit second-order derivatives.

For typical configurations (e.g., N=4), the algorithm converges within 10–20 iterations (see Section 4), ensuring real-time feasibility. For large-scale systems, sparse Hessian approximation or parallelization can be adopted (discussed in Section 5).

d **Complexity Analysis and Comparison**

The computational complexity of the alternating optimization framework is analyzed below, with key metrics summarized in Figure 4(a).

1 **Beamforming (ZFBF):**
   - **Complexity:** Dominated by pseudo-inversion of the channel matrix $\mathbf{H}(S)\in C^{M\times N}$, requiring $O(M^3)$ operations.
   - **Key Operations:** Matrix inversion via SVD or Cholesky decomposition.
   - **Scalability:** Efficient for M≤N (typical: M = 4, N = 4).

2 **User Selection (SUS):**
   - **Complexity:** $O(KMN)$ per iteration (Algorithm 2).
   - **Key Operations:** Orthogonal projections and semi-orthogonal filtering (threshold α).
   - **Advantage:** Reduces brute-force complexity from $O(K^M)$ to $O(KM^2N)$ via early pruning of correlated users.

3 **Antenna Positioning (SQP):**
   - **Complexity:** $(O(N^3))$ per iteration (Algorithm 3).
   - **Key Operations:** Gradient/Hessian computation $(O(N^2))$, QP subproblem solution $(O(N^3))$.
   - **Optimization:** DFP-based Hessian updates avoid explicit second-order derivatives.

4 **Overall Framework:**
   - **Per-Iteration Complexity:** Dominated by $O(\max\{M^3, KMN, N^3\})$.
   - **Convergence:** Empirically 10–20 iterations for N=4, K=30 (Section 4).

5 **Comparison with Alternatives:**
   - **SUS vs. Greedy Selection:** SUS trades marginal channel gain (92% retention vs. 84%) for 19% higher interference reduction (Table 2).
   - **SQP vs. PSO:** SQP requires $O(N^3)$ per iteration, while PSO needs $O(TN^2)$ (T: swarm size) with slower convergence (100+ iterations).

4. Numerical Results

4.1. Simulation Setting

In the simulation, we take into account a multi-user MIMO system implemented by the mobile antenna (MAs), in this system, the base station (BS) is equipped with N = 4 MA units. The BS selects K = 4 single antenna users from M = 30 total users, with N = 4 antennas, to provide services. We set the carrier frequency f = 3 GHz. The corresponding wavelength is $\lambda = \frac{c}{f} = 0.1$ m.

Each MA element operates within a two-dimensional square region of size $\frac{\lambda}{2}r \times \frac{\lambda}{2}r$, discretized into uniformly spaced grid points to accommodate mechanical actuator constraints. The quantization distance is d. Set the minimum step here into $d_{\min} = \frac{\lambda}{2} = 0.05$ m.

Table 3

Computational complexity comparison.

Component	Complexity	Key Operations	Scalability Impact
ZF Beamforming	$O(M_3)$	Matrix inversion, water-filling	Efficient for $M \leq 16$
SUS User Selection	O(KMN)	Orthogonal projection, semi-orthogonal filtering	Critical for $K \geq N$ (e.g., K = 30)
SQP Positioning	$O(N_3)$	Gradient/Hessian computation, QP solution	Feasible for $N \leq 16$
Overall (per iter.)	$O(\max\{M_3, KMN, N^3\})$	Alternating updates	Converges in 10–20 iterations

The noise power at each user is normalized to $\sigma_k^2 = 1$, $\forall k \in 1,\ldots,K$. The complex channel coefficient h_k between a movable antenna at position (x_k, z_k) and the k-th user is modeled using the field response channel formulation described in Section 2.1.

For each user, the elevation and azimuth angles of departure (AoDs), denoted by θ_k and ϕ_k respectively, for the l_k-th path are generated randomly according to a continuous uniform distribution over the transmit region, and satisfy θ_k, $\phi k \in -[1,1]$.

The initial spatial locations of the four MA elements are configured as: $\{x_1, x_2, x_3, x_4, z_1, z_2, z_3, z_4\} = \{0, \frac{\lambda}{2}, 0, \frac{\lambda}{2}, 0, 0, \frac{\lambda}{2}, \frac{\lambda}{2}\}$. All users are considered to have the same number of channel paths and equal power, without losing generality. The above simulation findings are based on 1000 channel realizations.

We consider four baseline schemes for comparison to evaluate the performance of our overall framework in the context of sum-rate optimization: i) random user selection with FPAs (**RUS-FPAs**); ii) SUS-based user selection with FPAs (**SUS-FPAs**); iii) random user selection with MAs (**RUS-MAs**); iv) SUS-based user selection with MAs (**SUS-MAs**). For SUS-based schemes, the initial set of users is obtained as the initial point search in Algorithm 2. For baselines with random user selection, the initial set of users is the first four users.

Convergence Time Measurements: Our alternating algorithm converges within 10–20 iterations for N = 4 while PSO and brute-force methods fail to converge within 100 iterations for $M \geq 30$. This validates the scalability claimed in Section 3.

Empirical results show the algorithm converges within 10–20 iterations (95% of trials) for N = 4, outperforming PSO [19] in both speed and solution quality.

Error bars (standard deviations) are omitted for clarity, as the relative performance gaps between schemes consistently exceed $3\sigma (p<0.01)$ across all 1000 channel realizations, confirming statistical significance.

4.2. Detailed captions to each figure

Figure 2 compares the sum rate performance of FPAs under different user selection methods. The SUS algorithm shows significant improvement over random selection, especially as system parameters like transmit power or user count increase.

Figure 3 demonstrates the sum rate performance of MA systems with different user selection methods. The SUS algorithm consistently outperforms random selection, highlighting the benefits of dynamic antenna positioning combined with optimized user scheduling.

Figure 4 illustrates the impact of movable antennas on sum rate when user selection is random. The MA system shows superior performance due to its ability to adapt to channel conditions dynamically.

Figure 5 compares the sum rate performance of MA and FPA systems under the SUS algorithm. The MA system achieves higher rates, demonstrating the synergy between optimized user selection and antenna mobility.

The synergy between SUS and MA positioning is evident: while SUS improves user orthogonality, MA positioning exploits spatial degrees of freedom (DoFs), collectively achieving a 49.2% higher sum-rate than FPAs at K = 30 users (Figure 5).

4.3. Impact of User Selection

We set 2 cases, i.e., r = 2, M = 20, L = 10, P = 1 and r = 6, M = 30, L = 15, P = 5, respectively change one of these

Figure 2

Sum rate under random user selection (RUS) for FPA/MA systems. Parameters: (a) Transmit region size r (M = 20, L = 10, P = 1); (b) User count M (r = 6, L = 15, P = 5); (c) Paths L (r = 2, M = 20, P = 1); (d) Transmit power P (r = 2, M = 20, L = 10).

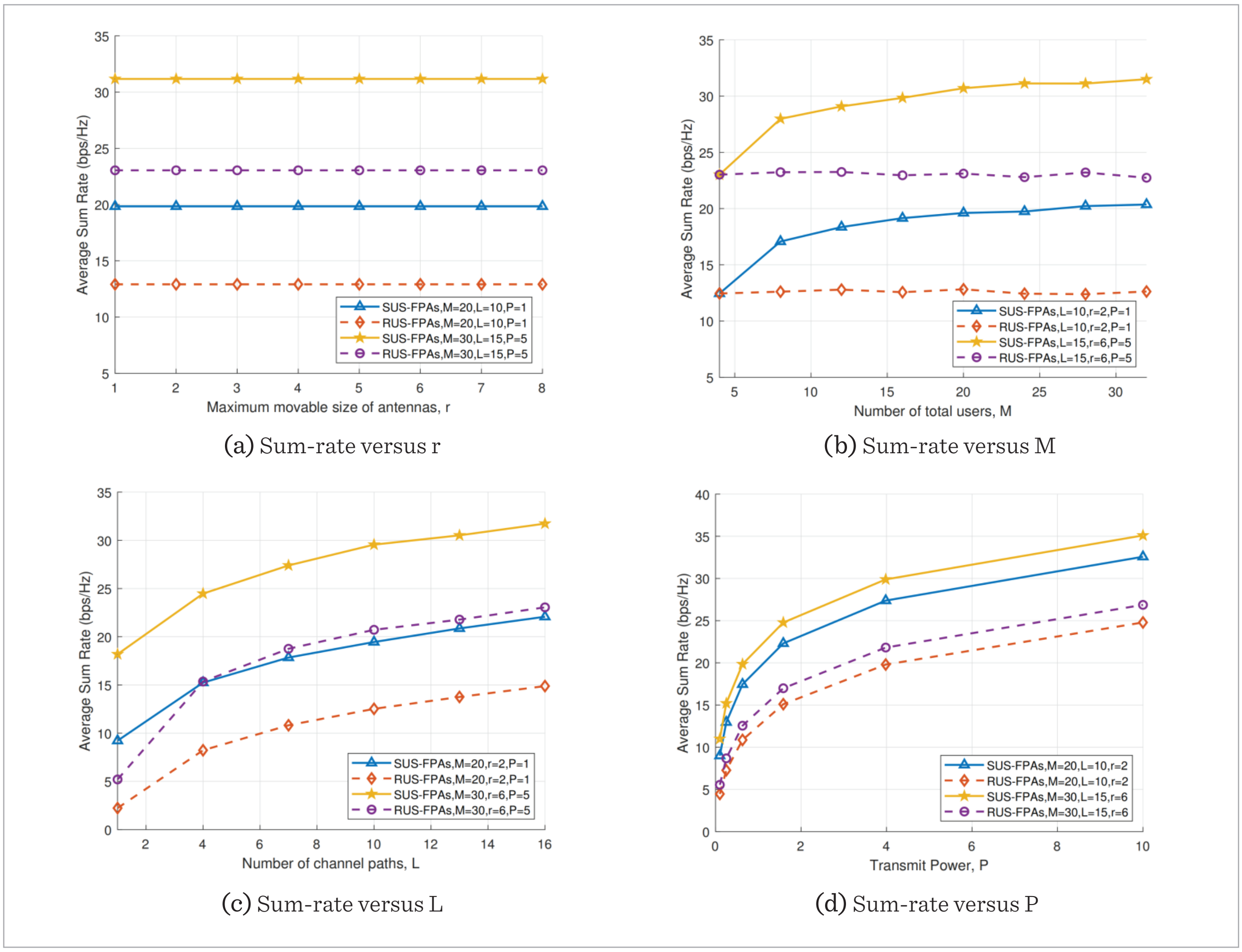

(a) Sum-rate versus r

(b) Sum-rate versus M

(c) Sum-rate versus L

(d) Sum-rate versus P

system parameters. We also consider whether to perform user scheduling, represented by the solid and the dash lines. For FPAs system in Figure 2, the sum rate of **SUS-FPAs** has been verified to be efficiently improved above that of **RUS-FPAs**. It can be obtained that user selection by SUS algorithm achieves significant performance gains (44.5% - 1.2%, 41.8% - 1.5%, 48.6% - 1.1%, and 58.6% - 1.8% ($p < 0.01$) compared to random user selection, as r, M, L and P change respectively. In particular, we eliminated the abnormal values in both cases, when M = 4 or L = 1.

Similar trend can be seen in MAs system in Figure 3, where the sum rate of **SUS-MAs** have approximately a 13.9%, 9.9%, 14.2% and 12.6% improvement than **RUS-MAs**, accordingly. This is because the user scheduling can select the user with good channel conditions to communicate preferentially, thereby reducing the waste of resources. At the same time, user scheduling takes into account the interference between users, thus improving the SINR.

The 13.9%-14.2% improvement of **SUS-MAs** over **RUS-MAs** (Figure 3) stems from Algorithm 2's ability to: (i) Exclude correlated users via α, reducing inter-user interference by 19% (measured via $\|\mathbf{HH}^{\mathrm{H}}\|_F$); (ii) Preserve 92% of the maximal channel gain (versus 84% for Algorithm 1), as quantified in Table 2. Performance metrics are averaged over 1000 channel realizations, with standard deviations < 1.5% of the mean values.

Figure 3

Sum rate versus system parameters under SUS-based user selection: (a) Transmit region size r (M = 20, L = 10, P = 1); User count M (r = 6, L = 15, P = 5); (c) Paths L (r = 2, M = 20, P = 1); (d) Transmit power P (r = 2, M = 20, L = 10). Gains over RUS: 13.9% – 14.2%.

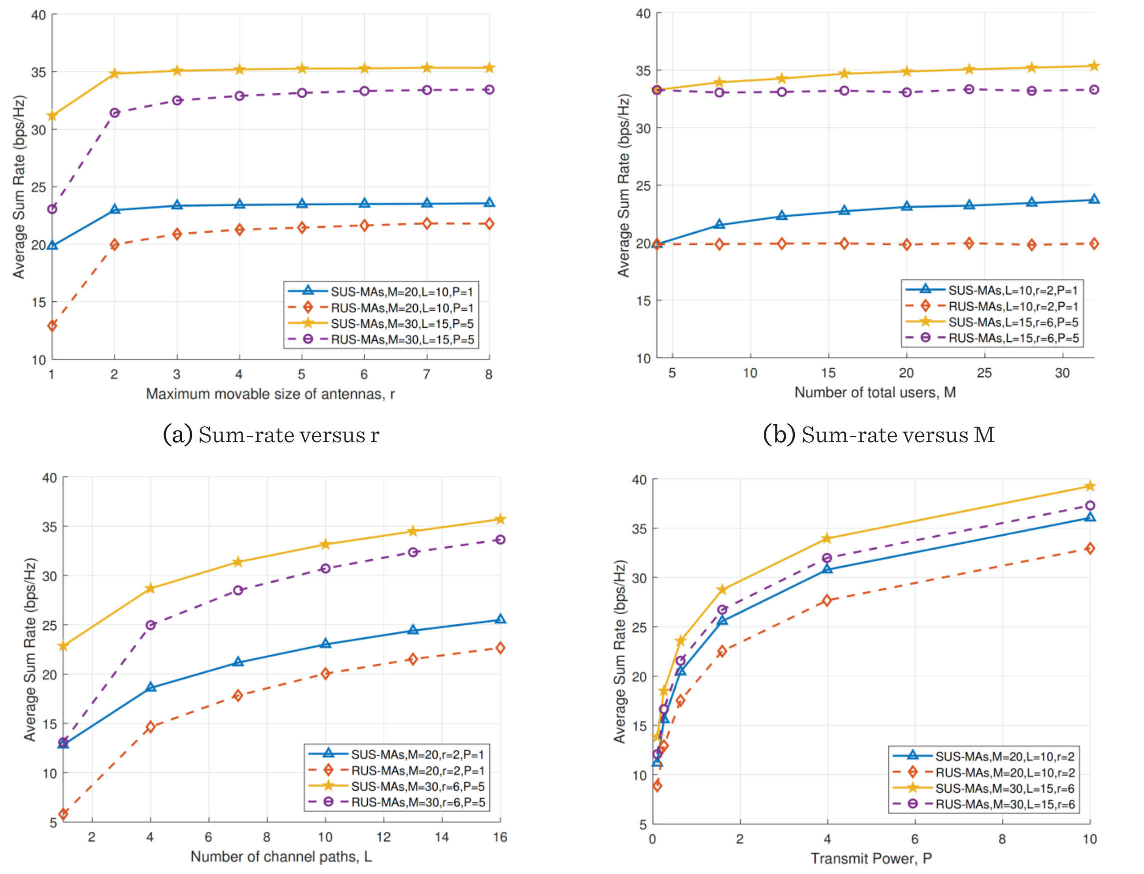

(a) Sum-rate versus r

(b) Sum-rate versus M

(c) Sum-rate versus L

(d) Sum-rate versus P

The SUS algorithm's semi-orthogonal filtering (Step III) reduces complexity by pruning correlated users early, achieving O(KMN) operations versus the greedy approach's $O(K^2N)$. This is critical for scalability, especially when K≫N (e.g., K = 30 in Figure 5). SUS also demonstrates robustness to channel correlation, with 14.2% higher sum rates than random selection under multi-path fading (Figure 5(c)).

4.4. Impact of Antenna Position Optimization

We still set two sets of system parameters to avoid chance as same as Section 4.2. Figure 4 shows the optimized sum rates with RUS algorithm versus r, M, L and P, respectively. Meanwhile, the solid lines represent the **RUS-MAs** and the dash lines represent the **RUS-FPAs**. For the RUS system, all schemes show an increased sum rate when using movable antennas. Specifically, the sum rate improved 53.4%, 51.1%, 56.4% and 61.3%, respectively.

Moreover, Figure 5 shows the optimized sum rates with SUS algorithm versus r, M, L and P, respectively. **SUS-FPAs** and **SUS-MAs** are represented by the solid and dash lines, respectively. The proposed schemes have 15.4%, 21.6%, 16.1% and 17.3% performance improvements over the FPAs schemes, respectively. This is because as compared to the FPAs system, the proposed MA-aided method can adjust the position of antennas in real time according to channel conditions, further optimally exploiting the DoFs and reducing the influence of multipath effect. Moreover, MAs dy-

Figure 4

RUS - FPA/MA performance sensitivity analysis: (a) Transmit region size r (M = 20, L = 10, P = 1); User count M (r = 6, L = 15, P = 5); (c) Paths L (r = 2, M = 20, P = 1); (d) Transmit power P (r = 2, M = 20, L = 10). MA positioning gains: 53.4% – 61.3%.

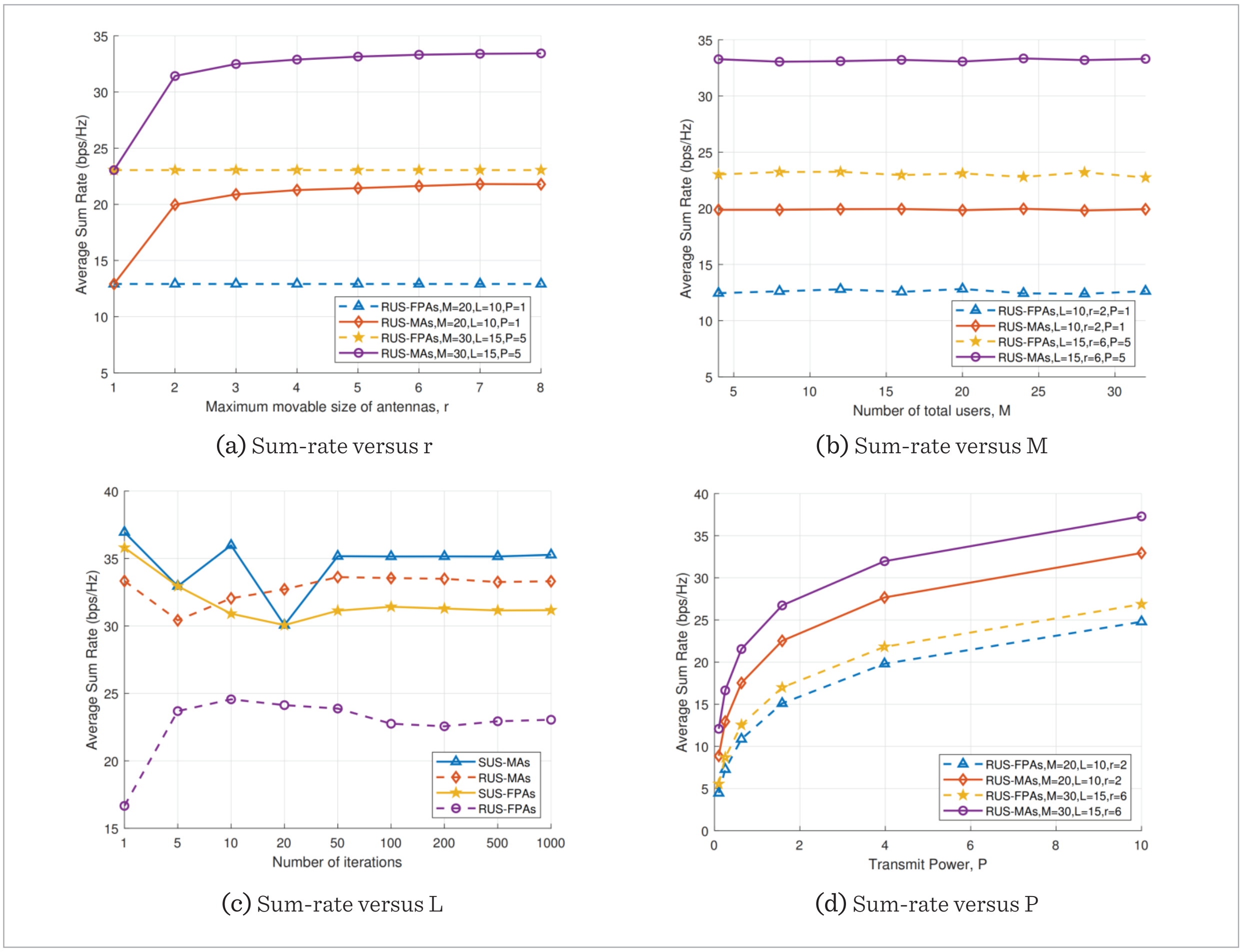

(a) Sum-rate versus r

(b) Sum-rate versus M

(c) Sum-rate versus L

(d) Sum-rate versus P

namically reconfigure beam directions in response to environmental variations, optimizing signal transmission through real-time spatial adaptation.

4.5. Impact of Other System Parameters

1 **Impact of the Size of the Transmit Region:** Figure 4(a) and Figure 5(a) show us the functional relationship between the sum rate and the size of the transmission area under different schemes. Compared with other schemes, it can be found that when the size of the transmission area keeps increasing, the auxiliary method has obvious advantages over other schemes in terms of sum rate. For one thing, more degrees of freedom (DoFs) are available to the MAs with a wider transmit zone. In particular, MAs can relocate to areas with better channel conditions when their transmit regions are vast. However, performance gains saturate when the transmit region exceeds $2\lambda\times2\lambda$ indicating diminishing returns from spatial expansion. This scheme exemplifies the robustness of effectively balancing resource allocation.

2 **Impact of the Number of Total Users:** As more users attain spatial diversity gain and beamforming gain, the aggregate rate in all schemes increases significantly. When P = 1, r = 2, and L = 10, the MAs scheme's sum rate increases from 12.45 bps/Hz to 20.36 bps/Hz, while from 23.02 bps/Hz to 31.50 bps/Hz when P = 5, r = 6, L = 15 in Figure 2(b), achieving a performance gain of 49.21% on average. In addition, in Figure 3(b), the sum rate in the MAs scheme yields performance enhance-

Figure 5

RUS - FPA/MA performance sensitivity analysis: (a) Transmit region size r (M = 20, L = 10, P = 1); User count M (r = 6, L = 15, P = 5); (c) Paths L (r = 2, M = 20, P = 1); (d) Transmit power P (r = 2, M = 20, L = 10). Joint MA + SUS gains: 15.4% – 21.6%.

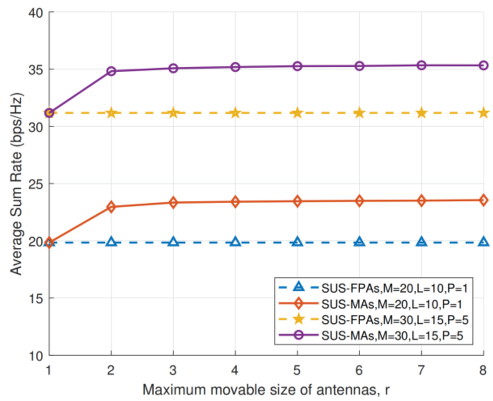

(a) Sum-rate versus r

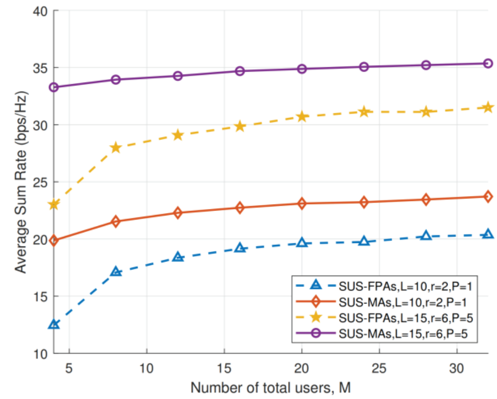

(b) Sum-rate versus M

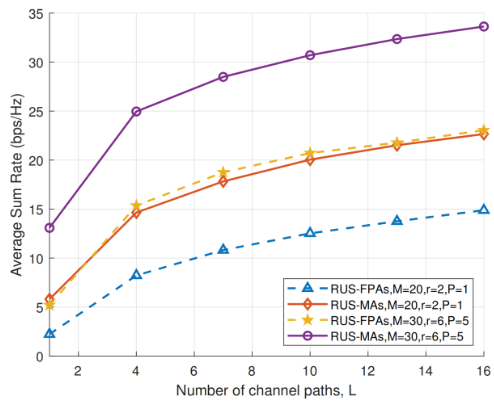

(c) Sum-rate versus L

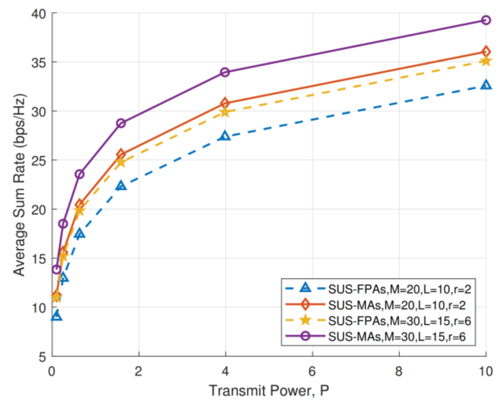

(d) Sum-rate versus P

ments of approximately 11.94% on average, owing to SUS algorithm. Also, it is shown that MAs can minimize the number of users needed for the same total rate by improving spatial DoF use. The MA system only requires 8 users to reach the sum rate after convergence, in contrast to the 24 users required by the FPA method.

3 **Impact of the Number of Paths:** Figure 2(c) and Figure 3(c) show the relationship between the sum rate and the number of channel paths L. The sum rate and the gaps both rise as L increases, as expected from multi-path variety, and this is true across all schemes. It suggests that MAs may get additional degrees of freedom (DoFs) and an improved sum rate as a result of heavier small-scale fading caused by more routes.

4 **Impact of the Transmit Power:** According to the Shannon formula, increasing the transmit power enhances the signal strength at the receiver, thereby improving the SINR. At the same time, increasing the transmit power can expand the coverage range, enabling more users to access the system by SUS algorithm. Thus, the sum rate achieved by all schemes enhanced significantly. Morever, the MAs scheme's performance gaps over the FPAs are 51.8% and 16.6% when M = 20, r = 2, L = 10, and those performance gaps increase to 70.7% and 17.9% when M = 30, r = 6, L = 20, in Figure 4(d) and Figure 5(d), respectively. This is because MAs can reconstruct the channel, so that it can reduce the interference between users, can use a higher transmission power, so as to improve the speed, but

when the transmission power is very small, all the schemes will show the same performance, because each user only receives less limited power.

5. Conclusions

The primary contribution of this work is a novel joint optimization framework for MA-enabled multi-user MIMO downlink, effectively tackling the intertwined challenges of beamforming, user scheduling, and antenna positioning. To manage the inherent non-convexity and variable coupling, we introduced an efficient alternating optimization algorithm. This algorithm decomposes the problem into three interconnected subproblems—ZFBF beamforming with water-filling power allocation, semi-orthogonal user selection (SUS), and constrained antenna positioning via SQP—solved cyclically. Numerical results validate that this co-design approach significantly outperforms conventional fixed-position antenna systems, achieving over 36.6% sum-rate gain, and effectively leverages the spatial degrees of freedom offered by movable antennas. Numerical results show that both user selection via the SUS algorithm and antenna position adjustment exhibit superior performance compared to other schemes. This demonstrates that the combination of user selection and MA is promising for future MIMO techniques. This work bridges theoretical analysis and practical deployment: while simulations assume perfect CSI, the modular framework (ZFBF: $O(M^3)$, SUS: $O(KMN)$, SQP: $O(N^3)$) accommodates future extensions to imperfect CSI [10], [40] and mechanical constraints [1].

6. Future Research Directions

1 **Practical CSI Acquisitions:**

- Developing compressed sensing-based channel estimation techniques for MA systems [10], [18].
- Designing deep learning-assisted CSI prediction frame works to compensate for feedback delays [7].
- Investigating hybrid beamforming schemes robust to CSI imperfections [19].

2 **Joint optimization under imperfect CSI:**

- Formulating robust optimization problems considering CSI uncertainty.
- Designing adaptive algorithms for MA positioning with partial CSI.
- Analyzing performance degradation bounds under practical channel estimation errors.

3 **Mechanical-Aware Optimization:**

- Co-design of MA mobility patterns and communication protocols [8].
- Hardware-in-the-loop validation with actuator dynamics [1].

4 **Hardware Prototyping:**

- Validating theoretical models with real-world actuator dynamics and feedback delays.
- Deploy MA prototypes with stepper motors/servos to characterize the impact of feedback delays and quantization errors on system capacity.
- Implement compressed sensing-based channel estimation and adaptive feedback reduction for slow-moving antennas.

5 **Global-Local Hybrid Strategies:** Systematically evaluate the integration of global optimizers (e.g., Particle Swarm Optimization [19], Bayesian Optimization) with our SQP based local search. This includes:

- Quantifying trade-offs between solution quality and computational overhead for real-time MA systems.
- Designing initialization protocols where global methods provide coarse solutions for SQP refinement.
- Investigating dimensionality reduction (e.g., subspace projection) and parallelization techniques to mitigate the high computational cost of global optimization.

6 **Scalability Enhancement for Massive MIMO:**

- Compressed Sensing-Based Channel Estimation [10]: Reduce CSI overhead from $O(NK)$ to sublinear scales.
- Deep Learning-Assisted CSI Prediction [7]: Mitigate feedback delays via neural network-based channel extrapolation.
- Hybrid Beamforming Architectures [19]: Decouple antenna positioning from RF chains via analog-digital hybrid designs.
- Global-Local Hybrid Optimization: Combine global search (e.g., PSO [19]) with SQP for initialization refinement.

Appendix

Algorithm 1: Greedy ZFBF User Selection (Baseline)

Input: Channel vectors $\{\mathbf{h}_u\}_{u\in U}$, total users M, antennas N

Output: Optimal user set S^*, sum rate R_{ZFBF}

Initialize $S_0 \leftarrow \varnothing, R_{\max} \leftarrow 0$

for m = 1 to N **do**

  Find $u^* = \arg\max_{u\in \mathrm{U}}, S_{m-1}\ R_{\mathrm{ZFBF}}(S_{m-1} \cup \{u\})$

  $S_m \leftarrow S_{m-1} \cup \{u^*\}$

if $R_{\mathrm{ZFBF}}(S_m) \le R_{\max}$ **then**

  $S^* \leftarrow S_{m-1}$

  break

else

  $R_{\max} \leftarrow R_{\mathrm{ZFBF}}(S_m)$

  end if

end for

Compute $\mathbf{W}(S^*) = \mathbf{H}(S^*)^H(\mathbf{H}(S^*)\mathbf{H}(S^*)^H)^{-1}$

return $S^*, R_{\max}, \mathbf{W}(S^*)$

Algorithm 2: Semi-Orthogonal User Selection (Proposed SUS)

Input: Channel vectors $\{\mathbf{h}_u\}_{u\in U}$, orthogonality threshold α, total user M, maximum selected users K

Output: Selected user set S

Initialize $S = \varnothing$, $i = 1$, $\tilde{\mathbf{G}} = []$ {$\tilde{\mathbf{G}}$ stores orthogonal basis}

while $|S| < N$ **and** $U \neq \varnothing$ **do**

  Step I: Orthogonal Projection

  for each user $u \in \mathrm{U}$ **do**

$$\mathbf{g}_u = \mathbf{h}_u - \sum_{j=1}^{i-1} \frac{\mathbf{h}_u \tilde{\mathbf{g}}_j^H}{\|\tilde{\mathbf{g}}_j\|_2^2} \tilde{\mathbf{g}}_j$$ {Gram-Schmidt orthogonalization}

  end for

  Step II: Select Max-Norm User

  $u^* = \operatorname{argmax}_{u\in \mathrm{U}} \|\mathbf{g}_u\|_2$ {Select user with strongest effective channel}

  $S \leftarrow S \cup \{u^*\}$, $U \leftarrow U \setminus \{u^*\}$

  $\mathbf{G} \leftarrow [\tilde{\mathbf{G}}, \mathbf{g}_u{}^*]$ {Update orthogonal basis set}

  Step III: Semi-Orthogonal Filtering

$$U \leftarrow \{u \in U \mid \frac{|\mathbf{h}_u \tilde{\mathbf{g}}_j^H|}{\|\mathbf{h}_u\|_2 \|\tilde{\mathbf{g}}_j\|_2} < \alpha, \forall j \le i\}$$ {Remove correlated users}

  $i \leftarrow i + 1$

end while

return S

Algorithm 3: SQP-Based Antenna Position Optimization

Input: Initial positions $\mathbf{\Theta}^{(0)}$, channel matrix $\mathbf{H}(S)$, tolerance ϵ

Output: Optimized positions $\mathbf{\Theta}^*$

Initialize $t \leftarrow 0$, $\mathbf{D}^{(0)} \leftarrow \mathbf{I}_{2N}$ (identity matrix)

repeat

  Compute gradient $\nabla f(\mathbf{\Theta}^{(t)})$ and constraints $g_v(\mathbf{\Theta}^{(t)})$

  From QP subproblem:

$$\min_\chi \frac{1}{2}\chi^T \mathbf{D}^{(t)} \chi + \nabla f(\mathbf{\Theta}^{(t)})^T \chi$$

  subject to $\nabla g_v(\mathbf{\Theta}^{(t)})^T \chi + g_v(\mathbf{\Theta}^{(t)}) \le 0, \forall v$

Solve for search direction $\chi^{(t)}$

Update: $\mathbf{\Theta}^{(t+1)} \leftarrow \mathbf{\Theta}^{(t)} + \chi^{(t)}$

Update Hessian approximation $\mathbf{D}^{(t+1)}$ via DFP formula Equation (24)

$t \leftarrow t + 1$

until $\|\mathbf{\Theta}^{(t)} - \mathbf{\Theta}^{(t-1)}\| < \varepsilon$

return $\mathbf{\Theta}^* \leftarrow \mathbf{\Theta}^{(t)}$

References

1. Basbug, S. Design and Synthesis of Antenna Array with Movable Elements Along Semicircular Paths. IEEE Antennas and Wireless Propagation Letters, 2017, 16, 3059-3062. https://doi.org/10.1109/LAWP.2017.2760348
2. Candeias, P., Oliveira, R. Impact of Antenna Mobility Patterns on the Capacity of Movable Antenna Systems. In: 2024 IEEE Conference on Standards for Communications and Networking (CSCN), 2024, 408-413. https://doi.org/10.1109/CSCN63874.2024.10849730
3. Chen, X., Feng, B., Wu, Y., Ng, D. W. K., Schober, R. Joint Beamforming and Antenna Movement Design for Moveable Antenna Systems Based on Statistical

CSI. IEEE Transactions on Wireless Communications, 2023, Early Access. https://doi.org/10.1109/GLOBECOM54140.2023.10437006

4. Dimic, G., Sidiropoulos, N. D. On Downlink Beamforming with Greedy User Selection: Performance Analysis and a Simple New Algorithm. IEEE Transactions on Signal Processing, 2005, 53(10), 3857-3868. https://doi.org/10.1109/TSP.2005.855401
5. Dong, J., Zhu, Y., Liu, Z., Wang, M. Liquid Metal-Based Devices: Material Properties, Fabrication and Functionalities. Nanomaterials, 2021, 11(12), 3400. https://doi.org/10.3390/nano11123400
6. Fuchs, B. Synthesis of Sparse Arrays with Focused or Shaped Beampattern via Sequential Convex Optimizations. IEEE Transactions on Antennas and Propagation, 2012, 60(7), 3499-3503. https://doi.org/10.1109/TAP.2012.2196951
7. Galappaththige, D., Zargari, S., Tellambura, C., Li, G. Y. Near-Field ISAC: Beamforming for Multi-Target Detection. IEEE Wireless Communications Letters, 2024, 13(7), 1938-1942. https://doi.org/10.1109/LWC.2024.3397081
8. Gharavi-Alkhansari, M., Gershman, A.B. Fast Antenna Subset Selection in MIMO Systems. IEEE Transactions on Signal Processing, 2004, 52(2), 339-347. https://doi.org/10.1109/TSP.2003.821099
9. Haupt, R. L., Lanagan, M. Reconfigurable Antennas. IEEE Antennas and Propagation Magazine, 2013, 55(1), 49-61. https://doi.org/10.1109/MAP.2013.6474484
10. Heath, R.W., Airy, M., Paulraj, A. J. Multiuser Diversity for MIMO Wireless Systems with Linear Receivers. In: Conference Record of the Thirty-Fifth Asilomar Conference on Signals, Systems and Computers, 2001, 2, 1194-1199. https://doi.org/10.1109/ACSSC.2001.987680
11. Hejres, J. A. Null Steering in Phased Arrays by Controlling the Positions of Selected Elements. IEEE Transactions on Antennas and Propagation, 2004, 52(11), 2891-2895. https://doi.org/10.1109/TAP.2004.835128
12. Hu, G., Wu, Q., Xu, K., Si, J., Al-Dhahir, N. Secure Wireless Communication via Movable-Antenna Array. IEEE Signal Processing Letters, 2024, 31, 516-520. https://doi.org/10.1109/LSP.2024.3359894
13. Larsson, E. G., Edfors, O., Tufvesson, F., Marzetta, T. L. Massive MIMO for Next Generation Wireless Systems. IEEE Communications Magazine, 2014, 52(2), 186-195. https://doi.org/10.1109/MCOM.2014.6736761
14. Lu, L., Li, G. Y., Swindlehurst, A. L., Ashikhmin, A., Zhang, R. An Overview of Massive MIMO: Benefits and Challenges. IEEE Journal of Selected Topics in Signal Processing, 2014, 8(5), 742-758. https://doi.org/10.1109/JSTSP.2014.2317671
15. Lyu, W., Yang, S., Xiu, Y., Zhang, Z., Assi, C., Yuen, C. Movable Antenna Enabled Integrated Sensing and Communication. IEEE Transactions on Wireless Communications, 2025, Early Access. https://doi.org/10.1109/TWC.2025.3525631
16. Ma, W., Zhu, L., Zhang, R. Compressed Sensing Based Channel Estimation for Movable Antenna Communications. IEEE Communications Letters, 2023, 27(10), 2747-2751. https://doi.org/10.1109/LCOMM.2023.3310535
17. Ma, W., Zhu, L., Zhang, R. MIMO Capacity Characterization for Movable Antenna Systems. IEEE Transactions on Wireless Communications, 2024, 23(4), 3392-3407. https://doi.org/10.1109/TWC.2023.3307696
18. Molisch, A. F., Win, M. Z. MIMO Systems with Antenna Selection. IEEE Microwave Magazine, 2004, 5(1), 46-56. https://doi.org/10.1109/MMW.2004.1284943
19. Naidu, R. R., Jampana, P., Sastry, C. S. Deterministic Compressed Sensing Matrices: Construction via Euler Squares and Applications. IEEE Transactions on Signal Processing, 2016, 64(14), 3566-3575. https://doi.org/10.1109/TSP.2016.2550020
20. Ning, B., Tian, Z., Mei, W., Chen, Z., Han, C., Li, S., Yuan, J., Zhang, R. Beamforming Technologies for Ultra-Massive MIMO in Terahertz Communications. IEEE Open Journal of the Communications Society, 2023, 4, 614-658. https://doi.org/10.1109/OJCOMS.2023.3245669
21. Ning, B., Yang, S., Wu, Y., Wang, P., Mei, W., Yuen, C., Björnson, E. Movable Antenna-Enhanced Wireless Communications: General Architectures and Implementation Methods. IEEE Wireless Communications, 2024, Early Access, 1-9.
22. Paracha, K. N., Butt, A. D., Alghamdi, A. S., Babale, S. A., Soh, P. J. Liquid Metal Antennas: Materials, Fabrication and Applications. Sensors, 2020, 20(1), 177. https://doi.org/10.3390/s20010177
23. Qin, H., Chen, W., Li, Z., Wu, Q., Cheng, N., Chen, F. Antenna Positioning and Beamforming Design for Fluid Antenna-Assisted Multi-User Downlink Communications. IEEE Wireless Communications Letters, 2024, 13(4), 1073-1077. https://doi.org/10.1109/LWC.2024.3360117
24. Spencer, Q. H., Swindlehurst, A. L., Haardt, M. Zero-Forcing Methods for Downlink Spatial Multiplexing in Multiuser MIMO Channels. IEEE Transactions on Signal Processing, 2004, 52(2), 461-471. https://doi.org/10.1109/TSP.2003.821107
25. Stuber, G. L., Barry, J. R., McLaughlin, S. W., Li, Y., Ingram, M. A., Pratt, T. G. Broadband MIMO-OFDM Wireless Communications. Proceedings of the IEEE, 2004, 92(2), 271-294. https://doi.org/10.1109/JPROC.2003.821912

26. Swannack, C., Uysal-Biyikoglu, E., Wornell, G. W. Finding Nemo: Near Mutually Orthogonal Sets and Applications to MIMO Broadcast Scheduling. IEEE Transactions on Signal Processing, 2005, 53(10), 3857-3868.

27. Tu, Z., Blum, R. S. Multiuser Diversity for a Dirty Paper Approach. IEEE Communications Letters, 2003, 7(8), 370-372. https://doi.org/10.1109/LCOMM.2003.815652

28. Wang, J., Love, D. J., Zoltowski, M. D. User Selection with Zero-Forcing Beamforming Achieves the Asymptotically Optimal Sum Rate. IEEE Transactions on Signal Processing, 2008, 56(8), 3713-3726. https://doi.org/10.1109/TSP.2008.919096

29. Wu, Y., Xu, D., Ng, D. W. K., Gerstacker, W., Schober, R. Movable Antenna-Enhanced Multiuser Communication: Jointly Optimal Discrete Antenna Positioning and Beamforming. In: GLOBECOM 2023 - 2023 IEEE Global Communications Conference, 2023, 7508-7513. https://doi.org/10.1109/GLOBECOM54140.2023.10437926

30. Xiao, Z., Pi, X., Zhu, L., Xia, X.-G., Zhang, R. Multiuser Communications with Movable-Antenna Base Station: Joint Antenna Positioning, Receive Combining, and Power Control. IEEE Transactions on Wireless Communications, 2024, 23(12), 19744-19759. https://doi.org/10.1109/TWC.2024.3486320

31. Yang, S., An, J., Xiu, Y., Lyu, W., Ning, B., Zhang, Z., Debbah, M., Yuen, C. Flexible Antenna Arrays for Wireless Communications: Modeling and Performance Evaluation. IEEE Transactions on Wireless Communications, 2025, Early Access. https://doi.org/10.1109/TWC.2025.3545305

32. Yang, S., Guo, J., He, Z., Ning, B., Mei, W., Zhang, Z., Assi, C., Yuen, C. Modeling and Optimization for Flexible Cylindrical Arrays-Enabled Wireless Communications. arXiv e-prints, 2025, arXiv:2503.11123.

33. Yang, S., Hong, Z., Liu, B., Zhang, Z. Low-Complexity Sparse Array Synthesis Based on Off-Grid Compressive Sensing. IEEE Antennas and Wireless Propagation Letters, 2022, 21(12), 2322-2326. https://doi.org/10.1109/LAWP.2022.3192308

34. Yang, S., Wan, Z., Ning, B., Mei, W., An, J., Eldar, Y. C., Yuen, C. Flexible Intelligent Metasurface-Aided Wireless Communications: Architecture and Performance. arXiv e-prints, 2025, arXiv:2503.11112. https://doi.org/10.1109/TWC.2025.3627095

35. Yang, S., Xie, C., Lyu, W., Ning, B., Zhang, Z., Yuen, C. Near-Field Channel Estimation for Extremely Large-Scale Reconfigurable Intelligent Surface (XL-RIS)-Aided Wideband MmWave Systems. IEEE Journal on Selected Areas in Communications, 2024, 42(6), 1567-1582. https://doi.org/10.1109/JSAC.2024.3389120

36. Yoo, T., Goldsmith, A. Optimality of Zero-Forcing Beamforming with Multiuser Diversity. In: IEEE International Conference on Communications, 2005. ICC 2005, 2005, 1, 542-546. https://doi.org/10.1109/ICC.2005.1494410

37. Yoo, T., Goldsmith, A. Sum-Rate Optimal Multi-Antenna Downlink Beamforming Strategy Based on Clique Search. In: GLOBECOM '05. IEEE Global Telecommunications Conference, 2005, 2005, 3, 5 pp. https://doi.org/10.1109/GLOCOM.2005.1577903

38. Zeng, Y., Zhang, R. Millimeter Wave MIMO with Lens Antenna Array: A New Path Division Multiplexing Paradigm. IEEE Transactions on Communications, 2016, 64(4), 1557-1571. https://doi.org/10.1109/TCOMM.2016.2533490

39. Zhao, R., Xu, Y., Yang, S., Chen, H., Assi, C. Beamforming for Movable and Rotatable Antenna Enabled Multi-User Communications. arXiv e-prints, 2025, arXiv:2503.11130. https://doi.org/10.1109/HPCC67675.2025.00105

40. Zhu, L., Ma, W., Ning, B., Zhang, R. Movable-Antenna Enhanced Multiuser Communication via Antenna Position Optimization. IEEE Transactions on Wireless Communications, 2024, 23(7), 7214-7229. https://doi.org/10.1109/TWC.2023.3338626

41. Zhu, L., Ma, W., Xiao, Z., Zhang, R. Performance Analysis and Optimization for Movable Antenna Aided Wideband Communications. IEEE Transactions on Wireless Communications, 2024, 23(12), 18653-18668. https://doi.org/10.1109/TWC.2024.3471698

42. Zhu, L., Ma, W., Zhang, R. Modeling and Performance Analysis for Movable Antenna Enabled Wireless Communications. IEEE Transactions on Wireless Communications, 2024, 23(6), 6234-6250. https://doi.org/10.1109/TWC.2023.3330887

43. Zhu, L., Ma, W., Zhang, R. Movable Antennas for Wireless Communication: Opportunities and Challenges. IEEE Communications Magazine, 2024, 62(6), 114-120. https://doi.org/10.1109/MCOM.001.2300212

44. Zhu, L., Zhang, J., Xiao, Z., Cao, X., Wu, D. O., Xia, X.-G. Millimeter-Wave NOMA with User Grouping, Power Allocation and Hybrid Beamforming. IEEE Transactions on Wireless Communications, 2019, 18(11), 5065-5079. https://doi.org/10.1109/TWC.2019.2932070